AGU PUBLICATIONS

Paleoceanography

RESEARCH ARTICLE
10.1002/2014PA002636

Key Points:
- Orbital-scale highs and lows in diatom paleoproductivity in the South Atlantic
- Unutilized Si and Fe fertilization actively drove Si uptake by diatoms
- Implications for diatom paleoproductivity and nutrient cycles

Correspondence to:
O. E. Romero,
oromero@uni-bremen.de

Citation:
Romero, O. E., J.-H. Kim, M. A. Bárcena, I. R. Hall, R. Zahn, and R. Schneider (2015), High-latitude forcing of diatom productivity in the southern Agulhas Plateau during the past 350 kyr, *Paleoceanography*, *30*, 118–132, doi:10.1002/2014PA002636.

Received 27 FEB 2014
Accepted 13 JAN 2015
Accepted article online 16 JAN 2015
Published online 21 FEB 2015

High-latitude forcing of diatom productivity in the southern Agulhas Plateau during the past 350 kyr

O. E. Romero[1], J.-H. Kim[2], M. A. Bárcena[3], I. R. Hall[4], R. Zahn[5], and R. Schneider[6]

[1]MARUM–Center for Marine Environmental Sciences, University of Bremen, Bremen, Germany, [2]Royal Netherlands Institute for Sea Research, Den Burg, Netherlands, [3]Department of Geology, Paleontology, Faculty of Sciences, University of Salamanca, Salamanca, Spain, [4]School of Earth and Ocean Sciences, Cardiff University College, Cardiff, UK, [5]Institució Catalana de Recerca I Estudis Avançats, Institut de Ciència I Tecnología Ambientals, Departament de Física, Universitat Autónoma de Barcelona, Barcelona, Spain, [6]Institut für Geowissenschaften, Universität Kiel, Kiel, Germany

Abstract The hydrography of the Indian-Atlantic Ocean gateway has been connected to high-latitude climate dynamics by oceanic and atmospheric teleconnections on orbital and suborbital timescales. A wealth of sedimentary records aiming at reconstructing the late Pleistocene paleoceanography around the southern African continent has been devoted to understanding these linkages. Most of the records are, however, clustered close to the southern South African tip, with comparatively less attention devoted to areas under the direct influence of frontal zones of the Southern Ocean/South Atlantic. Here we present data of the composition and concentration of the diatom assemblage together with bulk biogenic content and the alkenone-based sea surface temperature (SST) variations for the past 350 kyr in the marine sediment core MD02-2588 (approximately 41°S, 26°E) recovered from the southern Agulhas Plateau. Variations in biosiliceous productivity show a varying degree of coupling with Southern Hemisphere paleoclimate records following a glacial-interglacial cyclicity. Ecologically well-constrained groups of diatoms record the glacial-interglacial changes in water masses dynamics, nutrient availability, and stratification of the upper ocean. The good match between the glacial maxima of total diatoms concentration, *Chaetoceros* spores abundance, and opal content with the maximum seasonal cover of Antarctic ice and the atmospheric dust records points to a dominant Southern Hemisphere forcing of diatom production. Suborbital variability of SST suggests rapid latitudinal migrations of the Subtropical Front and associated water masses over the southern Agulhas Plateau, following millennial contractions and expansions of the subtropical gyres. Warmings of the upper ocean over site MD02-2588 during terminations IV to I occurred earlier than that in the Antarctic Vostok, which is indicative of a Northern Hemisphere lead. Our multiparameter reconstruction highlights how high-latitude atmospheric and hydrographic processes modulated orbital highs and lows in primary production and SST as triggered by northward transport of Si, eolian dust input, and latitudinal migrations of frontal zones.

1. Introduction

Oceanic frontal systems are of primary importance to the marine biota since their marked meridional gradients in physical and chemical properties strongly regulate the phytoplankton contribution to primary productivity [*Taylor and Ferrari*, 2011]. Frontal zones are crucial players in the ocean ecosystem of subpolar regions where the ocean absorbs large quantities of CO_2 from the atmosphere, thereby impacting the marine biological carbon pump and the global carbon cycle [*Read et al*., 2000]. Such frontal environments provide a unique location to explore the relationships between nutrient availability and the hydrographic and atmospheric controls over phytoplankton distribution and production and its contribution to the biological pump over different timescales.

The pronounced frontal system in the Indian-Atlantic Ocean gateway in the South Atlantic [*Peterson and Stramma*, 1991; *Belkin and Gordon*, 1996] consists of several circumpolar quasi-uniform belts divided by fronts, comparatively narrow zones of sharp changes in vertical structure, sea surface temperature (SST), salinity, and nutrient availability [*Orsi et al*., 1995]. These fronts are key components of the hydrography of the Indian-Atlantic Ocean gateway [*Lutjeharms*, 1996; *Orsi et al*., 1995; *Belkin and Gordon*, 1996] and create one of the most energetic regions of the world oceans [*Read et al*., 2000; *Graham and De Boer*, 2013], which are widely suggested to have potential implications for the global climate variability on a range of timescales [*Peeters et al*., 2004; *Martínez-Méndez et al*., 2010; *Marino et al*., 2013; *Simon et al*., 2013; *Ziegler et al*., 2013].

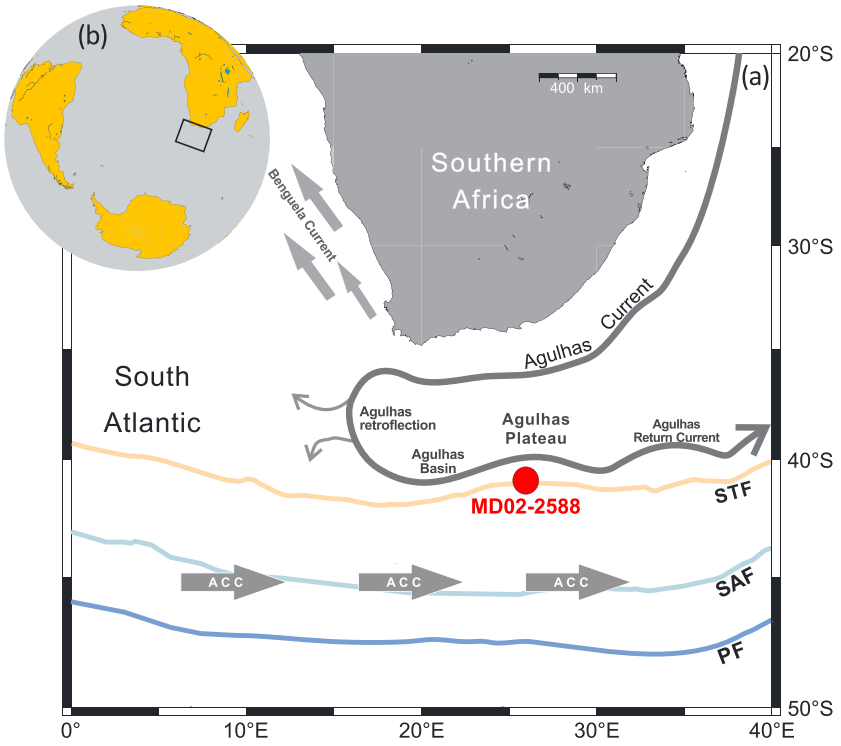

Figure 1. (a) Present-day location of fronts and large-scale circulation in the Southern Ocean and southern African sector. The red full circle represents the location of the MD02-2588 in the southern Agulhas Plateau. Full lines represent present-day average position of Subtropical (STF; light orange), Sub-Antarctic (SAF; light blue), and Polar (PF; ice blue) Fronts [after *Peterson and Stramma*, 1991; *Orsi et al.*, 1995]. The main path of the Agulhas Current, the Agulhas Retroflection, the Agulhas Return Current, and Antarctic Circumpolar Current (ACC, grey arrows) is also presented [*Lutjeharms*, 1996; *Peterson and Stramma*, 1991; *Orsi et al.*, 1995]. (b) The insert shows the Southern Ocean and the surrounding continents.

Because of water masses and wind dynamics, the Indian-Atlantic Ocean gateway is also a region of complex biogeochemistry [*Orsi et al.*, 1995] and phytoplankton spatial distribution and productivity variations [*Read et al.*, 2000] associated with the transition between the subtropical and sub-Antarctic domains.

The paleohydrography of the Indian-Atlantic Ocean gateway is suggested to have experienced a series of equatorward and poleward shifts of fronts and associated water masses following a glacial-interglacial cyclicity [e.g., *Flores et al.*, 1999; *Rau et al.*, 2002; *Peeters et al.*, 2004; *Bard and Rickaby*, 2009]. These studies were based on sediment cores mainly located within the main path of the Agulhas Current or under the direct influence of Agulhas leakage into the South Atlantic. In recent years, the paleoceanographic variability of intermediate and deep water masses around 40°S in the southern Agulhas Plateau has been addressed [*Diz et al.*, 2007; *Molyneux et al.*, 2007; *Martínez-Méndez et al.*, 2010; *Marino et al.*, 2013; *Simon et al.*, 2013; *Ziegler et al.*, 2013], hence closer to the present-day position of South Atlantic fronts [*Peterson and Stramma*, 1991; *Orsi et al.*, 1995]. *Ziegler et al.* [2013] studied the $\Delta\delta^{13}C$ signal recorded by deep-dwelling planktonic and benthic foraminifera and addressed the possible implications of fertilization by dust-borne iron on the efficiency of the biological pump in the southern Agulhas Plateau over the last 350 kyr. However, there remains a dearth of information on how the community of (siliceous) primary producers responded to varying gradients associated with the front migrations and changes in nutrient availability over the southern Agulhas Plateau for glacial-interglacial timescales. By using records of diatoms and the bulk biogenic content, we reconstruct productivity variations in surface waters of the southern Agulhas Plateau (site MD02-2588; Figure 1) for the past 350 kyr. In addition, a high-resolution record of alkenone-based SST allows insights into uppermost water column temperature. Being located at the present-day transition area between southern and northern originated water masses, site MD02-2588 allows us to test the potential effects of the physical-chemical nature of surface waters, the latitudinal migrations of fronts, and the possible effect of atmospheric dust/Fe input upon the variability of paleoproductivity in the southern Agulhas Plateau for the past 350 kyr.

2. Present-Day Conditions in the Indian-Atlantic Ocean Gateway

2.1. Fronts and Hydrography

The literature contains a wide range of suggested names and definitions of the Southern Ocean fronts. In this work, the use of front names and location follows *Peterson and Stramma* [1991] and *Orsi et al.* [1995, and references therein]. Pronounced meridional gradients in surface properties separate colder and fresher waters of the Southern Ocean from the warmer and saltier waters of the subtropical gyre circulations of the Southern Hemisphere. Present-day temperature and salinity distributions at 100 m indicate that the Subtropical Front (STF) (Figure 1), whose current location is determined by the regional wind field [*Matano et al.*, 1999], the latitudinal position of the southern westerlies, and the latitudinal extent of the subtropical gyres [*Sijp and England*, 2008], is located within a band across, whose surface temperature increases northward from 10°C to 12°C and salinities from 34.6 to 35.0 practical salinity unit (psu). Regardless of the season, SST (salinity) changes as large as 4–5°C (0.5 psu) mark the location of the STF; its northern side (~40°–39°S) is generally warmer (saltier) than 11.5°C (34.9 psu) [*Orsi et al.*, 1995]. More recently, *Graham and De Boer* [2013] reviewed the currently available definitions and climatologies of the STF and provided a new dynamical STF climatology based on maxima in satellite sea surface height gradients. *Graham and De Boer* [2013] suggest that the term STF only be used when referring to the surface water mass boundary.

The warmest water in the Indian-Atlantic Ocean gateway is Subtropical Surface Water (STSW), distinguished by temperature $>$ 23°C and relatively low salinities [*Gordon et al.*, 1987]. STSW extends southward to the Agulhas Retroflection Front (see below) with a wide range in characteristics (defined on the regional temperature-salinity relationship as 15°C, 35.5 psu to 24°C, 34.60 psu) [*Belkin and Gordon*, 1996]. South of the STF, the surface waters are carried by the Antarctic Circumpolar Current (ACC) (Figure 1) around the Southern Ocean and can be subdivided into distinct sub-Antarctic and Antarctic domains [*Holliday and Read*, 1998]. Sub-Antarctic Surface Water (SASW), found between the STF and the sub-Antarctic Front (SAF), has a wide range of temperatures and salinities varying with season (lower temperature in austral winter) and latitude (lower salinity south of the SAF) [*Belkin and Gordon*, 1996]. Although the SAF is less recognizable in the temperature field than in the salinity, it seems to coincide well with enhanced subsurface horizontal temperature gradients between 3° and 5°C isotherm [*Peterson and Stramma*, 1991]. The Polar Front (PF) is the northern boundary to cold ($-$1.5° to 2°C) near-surface water formed by winter cooling [*Peterson and Stramma*, 1991].

The Agulhas system comprises surface and intermediate water transport from the Indian Ocean into the Atlantic Ocean [*Belkin and Gordon*, 1996]. This transport takes place through the detachment of eddies and filaments from the Agulhas Retroflection, consisting of warm and salty Indian Ocean waters and providing a key return route for the supply of waters to the Atlantic Meridional Overturning Circulation [*Belkin and Gordon*, 1996]. The Agulhas Current is the largest surface western boundary current in the present-day global ocean transporting about 70 sverdrup of warm water along the southeastern African coast [*Bryden and Beal*, 2001]. Off the southern tip of South Africa, it undergoes a retroflection returning back into the South Indian Ocean and flows eastward as the Agulhas Return Current (Figure 1). In the retroflection area, warm water eddies spin off from the main current and drift westward into the South Atlantic Ocean contributing to the interplateau exchange of heat and salt between the Indian and South Atlantic Oceans [*Lutjeharms*, 1996]. The water mass between the Agulhas Retroflection Front and the STF has origins in Agulhas Water, Indian STSW, Atlantic STSW, and waters from the sub-Antarctic zone [*Belkin and Gordon*, 1996]. The Agulhas Return Current largely follows the STF, but occasionally, it separates between 13°E and 25°E to form a double front, comprising the Agulhas Front and the STF [*Belkin and Gordon*, 1996].

2.2. Productivity Patterns and Nutrient Availability

Highest surface chlorophyll *a* concentrations (range 0.5–0.8 mg m^{-3}) in the Indian-Atlantic Ocean gateway are found between the STF and SAF, reaching a maximum (1.25 mg m^{-3}) at the strongest convergence. Large planktonic diatoms (200–20 μm) are confined to discrete patches within the relatively high chlorophyll *a* STF region [*Read et al.*, 2000]. However, this fraction represents less than 20% of the total biomass for peak concentrations. Nannoplankton, typically characterized by thecate and athecate flagellates, dominates [*Read et al.*, 2000]. South of 45°S, chlorophyll *a* concentrations are typically $>$1 mg m^{-3}, and the Fe input via dust [*Martin*, 1990; *Mahowald et al.*, 1999] is responsible of the high export production of particulate organic carbon [*Schlitzer*, 2002].

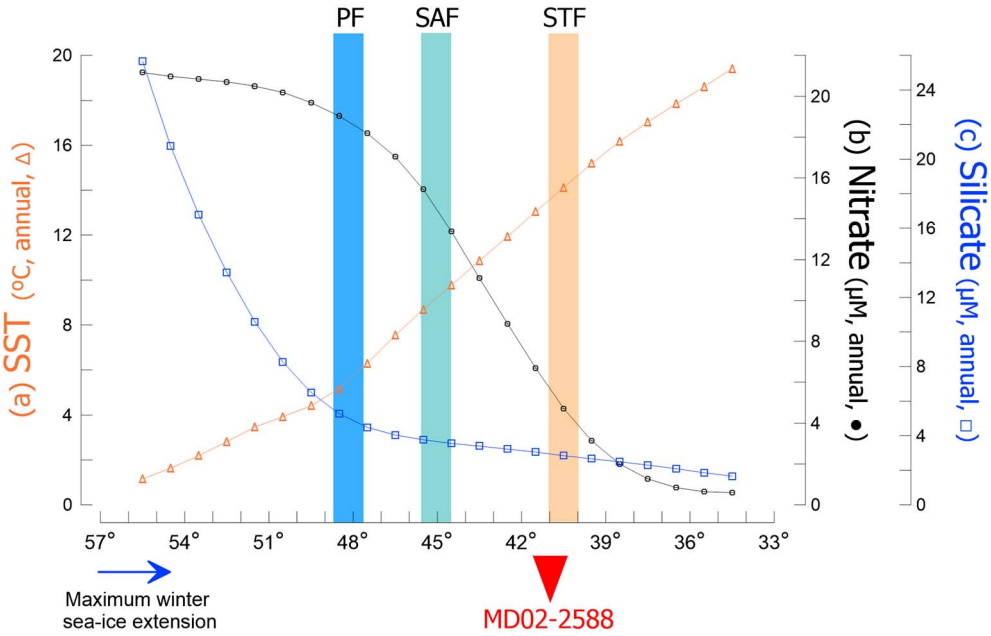

Figure 2. Present-day, annually averaged latitudinal values of (a) SST (°C, light brown line), (b) nitrate (μm, black line), and (c) silicate (μm, blue line) along 25°E in the Southern Ocean and the Indian-Atlantic Ocean gateway between 57° and 33°S off the southern tip of South Africa (LEVITUS94, http://iridl.ldeo.columbia.edu/SOURCES/.LEVITUS94/). The blue arrow indicates the maximal present-day extension of the winter Antarctic sea ice cover between 23° and 27°E. The inverted red triangle shows the location of site MD02-2588. References: SAF: Sub-Antarctic Front (light blue); STF: Subtropical Front (light orange bar); PF: Polar Front (dark blue bar) [after *Peterson and Stramma*, 1991; *Orsi et al.*, 1995].

Maximum chlorophyll *a* concentrations fall between 10° and 17°C (SST) and coincide with minimum silicate values ($<3\ \mu mol\ L^{-1}$) but nonlimiting nitrate concentrations (Figure 2), characteristic of modified SASW between the STF and the SAF. In warmer STSW (>17°C), low chlorophyll *a* is associated with minimum nitrate and silicate concentrations of up to $2\ \mu mol\ L^{-1}$. However, in cold SASW (<10°C, south of 51°S), low chlorophyll *a* is associated with maximum nitrate and silicate concentrations.

Present-day (interglacial) diatom production in the southern Agulhas Plateau is limited by the Si availability because little of the dissolved Si south of the PF survives in SASW long enough to be transported northward across the SAF [*Brzezinski et al.*, 2002; *Matsumoto et al.*, 2002]. As shown by their current distribution, a sharp decrease in annual Si and N content occurs at the SAF (approximately 48°S, Figure 2). The supply of Si does not follow a linear relationship with N and P. Nutrients are presently supplied to the Indian-Atlantic Ocean gateway by Southern Hemisphere winds [*Mahowald et al.*, 1999; *Kohfeld et al.*, 2005, and references therein], the wind-driven northward transport of nutrient-rich SASW, and by lateral mixing from the south rather than by the upwelling from intermediate and deeper water masses [*Sigman et al.*, 1999].

3. Material and Methods

3.1. Core MD02-2588

Calypso giant box core MD02-2588 (10.65 m) was retrieved during RV *Marion Dufresne* cruise MD128 in 2002 at 2907 m water depth on the southwestern flank of the Agulhas Plateau (41°19.9′S; 25°49.7′E, Figure 1). The sediment core was recovered from a contourite sediment drift that closely follows the morphology of the plateau [*Uenzelmann-Neben*, 2002]. Sediments of core MD02-2588 are mostly light gray colored with slightly bioturbated, silty clay.

3.2. Age Model

The MD02-2588 age model was established by *Ziegler et al.* [2013]. The age scale is constrained in the upper section (<40 kyr) by 15 calibrated accelerator mass spectrometry ^{14}C dates, on monospecific samples of the planktonic foraminifera *Globigerina bulloides* and *Globorotalia inflata*. ^{14}C measurements were carried out at

the Scottish Universities Environmental Research Centre Accelerator Mass Spectrometer Laboratory. Conventional ages between 115 and 130 cm are older than ~40 ka, i.e., beyond the laboratory ^{14}C dating limit, and therefore were not considered in the age model [*Ziegler et al*., 2013]. Beyond ^{14}C dating control, between 105 and 1070 cm, a graphical correlation of the benthic $\delta^{18}O$ record to the European Project for Ice Coring in Antarctica (EPICA) DomeC δD record was performed. The resulting age model allows direct comparison of the MD02-2588 data with those gained in Antarctica. The correlation also results in a good match between the MD02-2588 benthic $\delta^{18}O$ and the global benthic $\delta^{18}O$ stack LR04 [*Lisiecki and Raymo*, 2005] with only a few minor exceptions, which are related to the differences of the age model constructions of both records [*Ziegler et al*., 2013]. Core MD02-2588 reaches marine oxygen isotope stage (MIS) 10 at its base, and its average sedimentation rate is 3.4 cm kyr^{-1} [*Ziegler et al*., 2013].

3.3. Sample Preparation and Analysis

3.3.1. Diatoms

Diatom studies were carried out on samples spaced every 10 cm. Samples were prepared according to the standard randomly distributed microfossils method of *Schrader and Gersonde* [1978]. Qualitative and quantitative analyses were carried out on permanent slides of acid-cleaned material (*Permount*® mounting medium) at 1000X magnifications using a Leica DMLB with phase contrast illumination (Department of Geology, Paleontology, University of Salamanca, Spain). The counting methodology of valves followed *Schrader and Gersonde* [1978]. Several traverses across each cover slip were examined, depending on diatom abundances (between 350 and 700 valves were counted for each cover slip). Two cover slips per sample were scanned in this way. In order to have a statistically significant amount of valves, a second counting was done for samples with high amounts of *Chaetoceros* resting spores (RS) (MIS2–4, MIS6, MIS8, and late MIS10).

3.3.2. Bulk Geochemistry

Total carbon (TC) contents were measured on untreated samples, taken every 2 cm. After decalcification with 2 N HCl, the total organic carbon (TOC) content was obtained by combustion at 1050°C using a Heraeus CHN-O-Rapid elemental analyzer [*Müller et al*., 1994]. Carbonate was calculated from the difference between TC and TOC and expressed as calcite ($CaCO_3 = (TC - TOC) \times 8.33$). Opal content, measured every 5 cm, was determined by the sequential leaching technique by *De Master* [1981], with modifications by *Müller and Schneider* [1993]. The precision of the analytical system for opal is better than 0.5% [*Müller and Schneider*, 1993].

3.3.3. Alkenone Analysis and SST Estimations

To determine past SST variations, alkenones were extracted from 1–2 g sediments from freeze-dried and homogenized samples taken every 2 cm, following *Kim et al*. [2002]. The extracts were analyzed by capillary gas chromatography using a gas chromatograph (HP 5890A) equipped with a 60 m column (J&W DB1, 0.32 mm × 0.25 μm), a split injector (1:10 split modus), and a flame ionization detector. Quantification of the alkenone content was achieved using squalane as an internal standard. The alkenone unsaturation index $U^{K'}_{37}$ was calculated from $U^{K'}_{37} = (C_{37:2})/(C_{37:2} + C_{37:3})$ as defined by *Prahl and Wakeham* [1987], where $C_{37:2}$ and $C_{37:3}$ are the di-unsaturated and tri-unsaturated C_{37} methyl alkenones. The $U^{K'}_{37}$ values were converted into temperature values applying the culture calibration of *Prahl et al*. [1988] ($U^{K'}_{37} = 0.034 \times T + 0.039$), which has also been validated by core top compilations [*Müller et al*., 1998]. The precision of the measurements ($\pm 1\sigma$) was better than 0.003 $U^{K'}_{37}$ units (or 0.1°C), based on multiple extractions and analyses of a sediment sample used as a laboratory internal reference from the South Atlantic.

4. Ecology of Diatoms in the Southern Agulhas Plateau

Due to the high diversity of the MD02-2588 diatom assemblage, and in order to summarize the paleoecological information delivered by the main contributors, diatoms were grouped according to their modern and late Quaternary ecological preferences. All identified diatom species with well-known ecological requirements were assigned to one of the following three groups: (a) resting spores (RS) of *Chaetoceros*, (b) the tropical/subtropical assemblage, and (c) pelagic Southern Ocean diatoms (SODs).

In middle and high latitudes, RS of *Chaetoceros* occur in high-productivity and low-temperature waters [*Smetacek*, 1999; *Armand et al*., 2005; *Romero and Armand*, 2010]. Because *Chaetoceros* RS preserve better than its thin-walled vegetative cells in regions of major organic carbon export but of low-to-moderate opal deposition [*Smetacek*, 1999], the spores are robust indicators of presence or absence of high carbon, low silica

exporting phytoplankton blooms. The molar Si:N demand of *Chaetoceros* is close to 1. The tropical/subtropical assemblage characterizes the occurrence of temperate-to-warm, mesotrophic-to-oligotrophic waters and includes at site MD02-2588 several well-silicified taxa such as *Alveus marinus*, *Azpeitia* spp., *Fragilariopsis doliolus*, *Hemidiscus cuneiformis*, *Roperia tesselata*, and several varieties of *Thalassionema nitzschioides*—except varieties of *nitzschioides* and *Thalassiosira ferelineata* [*Romero et al*., 2005; *Romero and Armand*, 2010].

The pelagic SOD group [*Armand et al*., 2005; *Crosta et al*., 2005] is mainly composed of the open ocean diatoms *Fragilariopsis kerguelensis*, typical of high southern latitudes, with minor contribution of *Eucampia antarctica*, *Thalassiosira antarctica*, *Thalassiosira gracilis*, and *Thalassiosira lentiginosa*. A prominent member of the large-celled, heavily silicified (Si:N approximately 2–6) diatom assemblage characteristic of the Fe-limited ACC [*Smetacek*, 1999], *F. kerguelensis* reaches peak abundance in the permanent open ocean zone south of the PF, while its distribution is constrained by low Si north of the PF [*Zielinski and Gersonde*, 1997; *Fischer et al*., 2002]. The dissolution-resistant *F. kerguelensis* dominates the diatom community preserved in late Quaternary sediments of the Southern Ocean silica belt below the present-day path of the ACC [*Cortese and Gersonde*, 2007, and references therein].

In addition to the three main diatom groups, we also identified several coastal planktonic as well as shallow-water, benthic diatoms, altogether contributing with less than 2% to the total diatom assemblage. These two groups are not discussed here.

5. Results

5.1. Total Diatom Concentration

The total diatom concentration varied strongly (range 3.1×10^5–1.3×10^7 valves g^{-1}, average = 2.4×10^6 valves $g^{-1} \pm 1.2 \times 10^6$). During the past 350 kyr, intervals of maxima and minima mainly followed a glacial/interglacial pattern: highest values (8.0×10^6–1.2×10^7 valves g^{-1}) were reached during MIS4–MIS2, while lowest ($<4.0 \times 10^6$ valves g^{-1}) occurred during MIS7, MIS5, and from late MIS1 into the Holocene (Figure 3a). Absolute differences of the total diatom concentration between glacials were more pronounced between 190 kyr and the late Holocene than earlier between 350 and 190 kyr (Figure 3a).

5.2. Diatom Groups

For the entire studied period, the highest average relative contribution correspond to tropical/subtropical diatoms (26.6% ± 9.04, range 63.5–7.3%), followed by spores of *Chaetoceros* (24.3% ± 21.51; range = 75.5–1.0%) and the pelagic SOD (15.1% ± 9.8; range = 47.0–1.2%). The contribution of the two main diatom groups—tropical/subtropical and RS *Chaetoceros* (total common average = approximately 52%)—followed a glacial/interglacial pattern of variation (Figures 3b and 3c). The contribution of tropical/subtropical diatoms was highest during interglacials: up to approximately 64% of the total diatom assemblage during MIS5 and between 20 kyr and the late Holocene. Highest abundances of RS *Chaetoceros* occurred during MIS6, MIS4, and between MIS3 and MIS2, with minor peaks during late MIS10 and early MIS8. Pelagic SOD peaked during terminations (T) III and II with moderate maxima during MIS9 and TI (Figure 3d).

5.3. Bulk Biogenic Contents

For the past 350 kyr, calcium carbonate ($CaCO_3$) dominated (60–87%) the bulk biogenic production at site MD02-2588, followed by opal (biogenic silica) and TOC (Figure 4). The content of $CaCO_3$ reached highest values during interglacials (Figure 4a). $CaCO_3$ values increased shortly after the beginning of each interglacial, decreased toward the middle interglacial stage, to increase again in the second half of each interglacial. $CaCO_3$ content decreased during the early part of full glacials (MIS8, MIS4, and MIS2) and increased abruptly afterward (e.g., around 268, 64, and 19 kyr) toward the end of the glacial. Opal values ranged from 0.5 to 2.4 wt % (Figure 4b). Opal content peaked during MIS10, MIS8, MIS6, and MIS4 and between MIS3 and MIS2, while it was lower during interglacials MIS5, early MIS3, and shortly after the Last Glacial Maximum. TOC content was low (range = 0.13–0.61 wt %) (Figure 4c). In spite of the lower resolution of the opal measurements compared to those of TOC, the glacial/interglacial pattern of opal matched well with that of TOC. Opal and TOC varied strongly on both the orbital and suborbital scales.

5.4. Alkenone Concentration and Estimated SST

The alkenone concentration varied between 50 ng cm^{-2} and 2238 ng g^{-1} (average = 834 ± 460 ng g^{-1}) and displayed prominent fluctuations on both orbital and suborbital timescales (Figure 4d). Highest alkenone

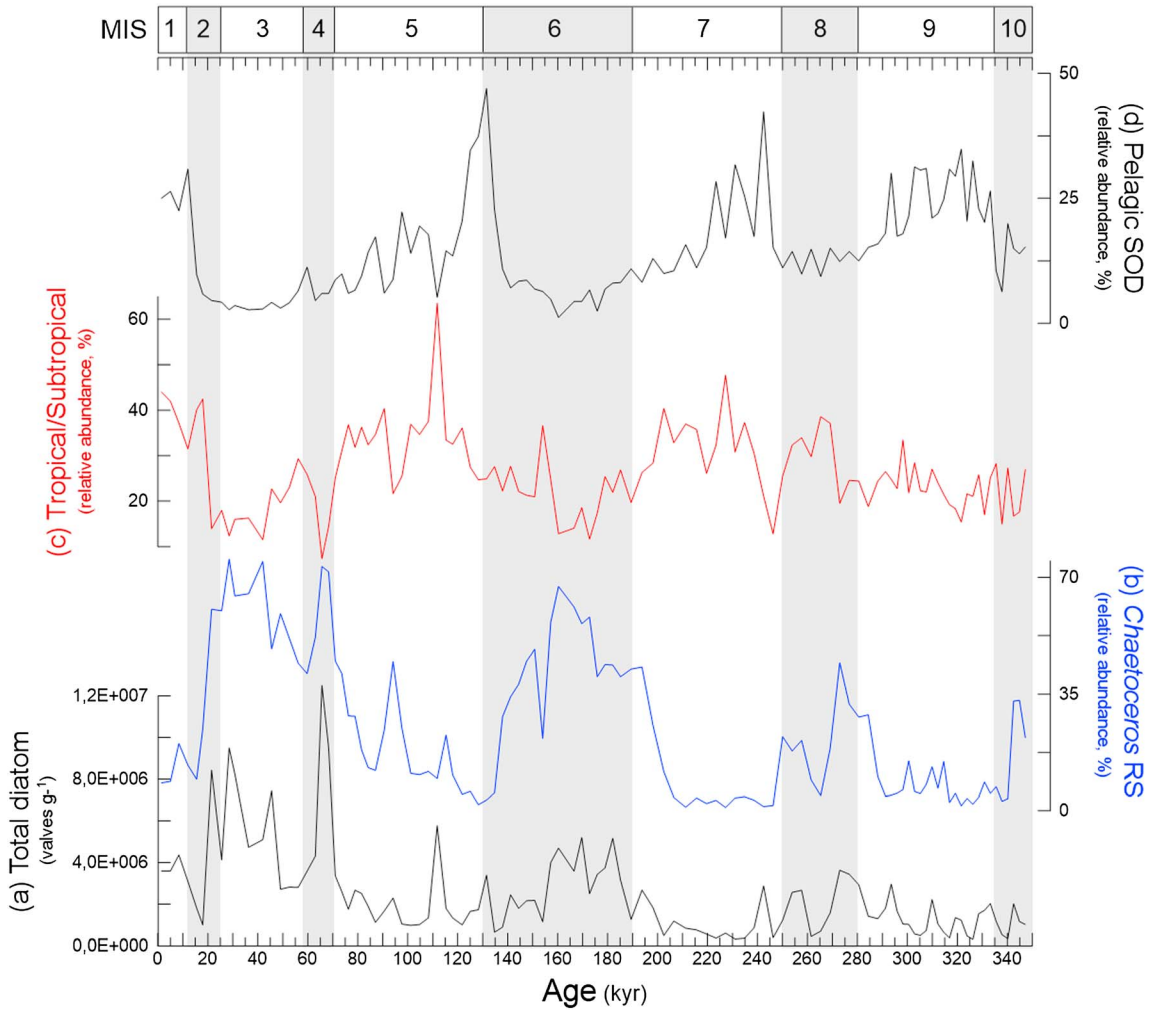

Figure 3. Concentration of (a) total diatoms (valves g^{-1}; black line) and relative contribution (%) of diatom groups, (b) resting spores (RS) of *Chaetoceros* (blue line), (c) tropical/subtropical diatoms (red line), and (d) pelagic Southern Ocean diatoms (SOD, black line) at site MD02-2588 for the last 350 kyr. Vertical light grey shadings indicate glacials (numbers in box indicate marine oxygen isotope stages—MIS—1 to 10).

values occurred mostly during glacials, while interglacials recorded mostly the lowest values. Alkenone concentration was mostly above average during MIS10, MIS8, and MIS6. The temporal dynamics and lowest and highest of SST, however, differ among isotope stages. Values during MIS3 were closer to those of MIS6 than to any full interglacials during the last 350 kyr. The lowest concentration of alkenones is recorded between late MIS2 and late MIS1.

The alkenone-derived SSTs varied between 11.3° and 22.3°C (average = 17.4 ± 1.84°C) and displayed prominent fluctuations on both orbital and suborbital timescales (Figure 4d). Highest SSTs occurred mostly during interglacials, while glacials recorded mostly the lowest values for the entire study period. SSTs were mostly below average during glacials, while only during MIS7 and MIS5 raised above average. The temporal dynamics and lowest and highest of SST, however, differ among isotope stages.

SSTs ranged mostly between 15.3 and 22.3°C during interglacials (modern range = 13.6–16.4°C). MIS9 had highest values between 330 and 320 kyr, while SSTs remained below the average until the end of stage. MIS7 and MIS5 were warmer than MIS9, and SST amplitude was higher during MIS5 than MIS7. Values during MIS3 were closer to those of MIS6 than to any full interglacials during the last 350 kyr. The SST timing of highs and lows during MIS5 followed a different pattern than that of MIS9 and MIS7: after reaching highest SST maxima for the entire study period during TII (136–130 kyr), SST diminished from ~22°C around 124 kyr down to 17.4°C at 112 kyr. The SST decrease between approximately 60 and 40 kyr was followed by an increase of 2.3°C between 40.9 and 39.4 kyr.

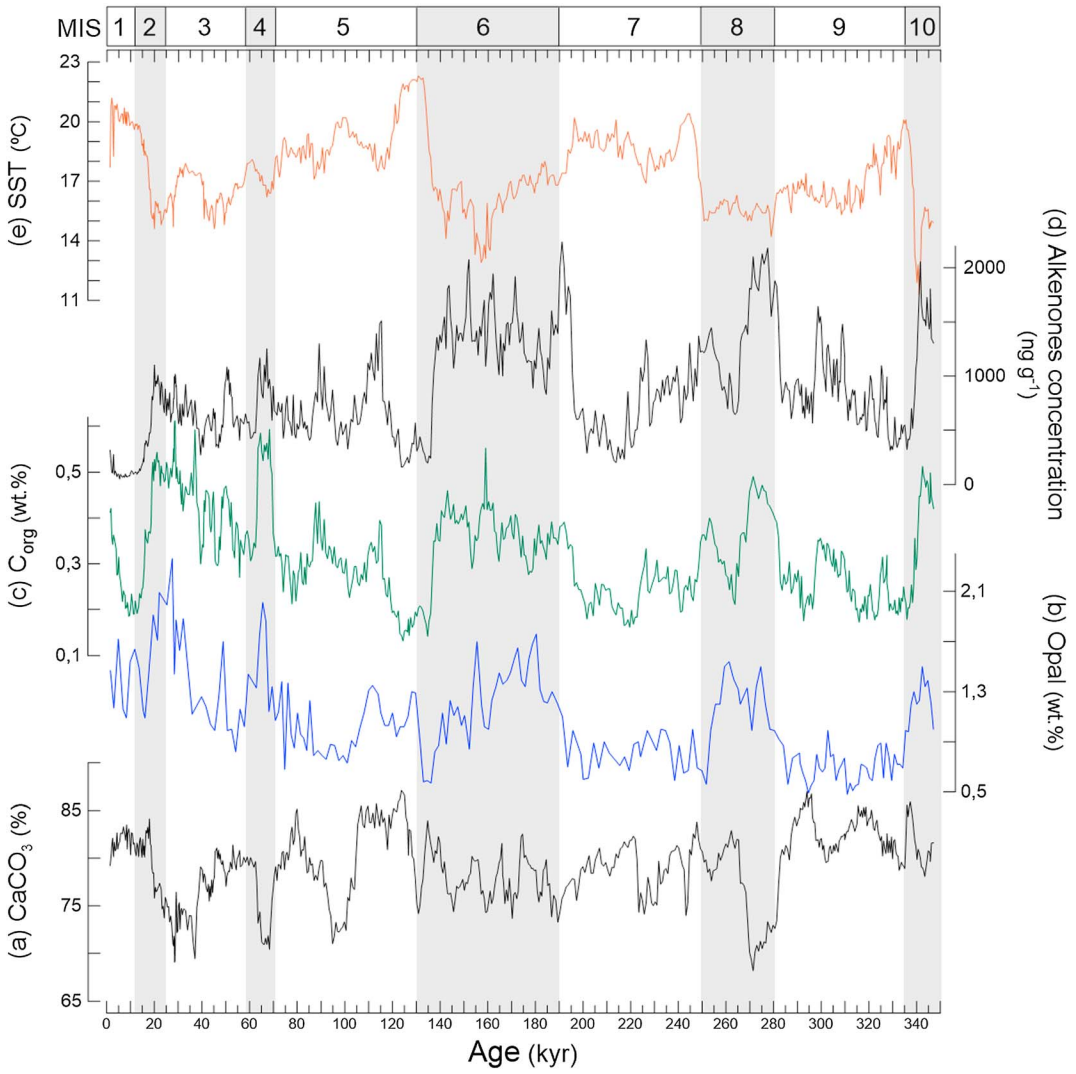

Figure 4. Concentration of (a) calcium carbonate ($CaCO_3$, %; black line), (b) opal (biogenic silica, wt %, blue line), (c) total organic carbon (C_{org}, %; green line), (d) alkenone concentration (ng g^{-1}, black line), and (e) alkenone-based SST (°C; light brown line) at site MD02-2588 for the last 350 kyr. Vertical light grey shadings indicate glacials (numbers in box indicate marine oxygen isotope stages—MIS—1 to 10).

Low SSTs occurred during full glacials (late MIS10, 11.3°C, 341 kyr; middle MIS6, 13.3°C, 154.7 kyr). SST minima occurred between 330 and 340 kyr (late MIS10) and 161–148 kyr (middle MIS6). Compared to MIS8 and MIS4–MIS2, MIS6 also recorded the widest range of SST amplitude.

6. Discussion

Total diatom concentration and bulk biogenic values at site MD02-2588 mainly followed an orbital-scale pattern of variability for the past 350 kyr. The combined effect of nutrient availability, mixing of the uppermost water column, and atmospheric and hydrography variations in the Southern Ocean and the South Atlantic defined the pattern of diatom production at site MD02-2588.

6.1. Southern Hemisphere-Driven Inputs of Nutrients Into the Southern Agulhas Plateau

For the past 350 kyr, the glacial/interglacial variability of diatoms and bulk biogenic components at site MD02-2588 are interpreted to reflect orbital-scale variations in paleoproductivity occurred in surface waters of the southern Agulhas Plateau. Since the present-day pronounced meridional gradient in surface properties south of 38°S are influenced by the latitudinal contractions and expansions of the subtropical gyres and

thesurface water masses reaching the study area [*Matano et al*., 1999; *Sijp and England*, 2008], we propose that the latitudinal migration of the closely located fronts and the shifts in the nutrient availability determined the pattern of variations of diatom and bulk content at site MD02-2588.

Nutrients are presently supplied to the southern Agulhas Plateau by Southern Hemisphere winds [*Kumar et al*., 1995; *Mahowald et al*., 1999; *Kohfeld et al*., 2005] and by lateral mixing from intermediate water masses of southern origin [*Sigman et al*., 1999]. Low present-day Si availability limits diatom production in the study area (see section 2.) The northward transport of Si depends on its uptake and availability south of the PF and the extent of the Antarctic ice cover. A larger winter sea ice cover during late Quaternary glacials [*Gersonde et al*., 2003; *Crosta et al*., 2004] limited the diatom production south of the PF, causing the unutilized pool of H_4SiO_4 to be advected into Atlantic midlatitudes [*Brzezinski et al*., 2002; *Matsumoto et al*., 2002; *Sarmiento et al*., 2004]. This excess of H_4SiO_4 might have been transported by Sub-Antarctic Mode Waters (SAMW, much as nitrate is today [*Sigman et al*., 1999]) to the thermocline of the southern Agulhas Plateau [*Sarmiento et al*., 2004]. We postulate that the northward migration of SAF and STF and associated water masses during full glacials [*Mortlock et al*., 1991; *Kumar et al*., 1995; *Flores et al*., 1999; *Rau et al*., 2002; *Peeters et al*., 2004; *Marino et al*., 2013; *Simon et al*., 2013] drew the Southern Ocean originated nutrient source closer to waters over site MD02-2588, thus alleviating the Si limitation of surface waters overlying the southern Agulhas Plateau (Figure 2) and helped diatoms, well known for their limited motility [*Smetacek*, 1999], to increase their productivity.

With Si—but no Fe—being supplied to waters to the north of the PF during full glacials, diatoms in the southern Agulhas Plateau would have been unable of building new valves. The effect of bioavailable Fe limitation in slowing down diatom production and in changing their Si:N uptake ratios has been demonstrated both by culturing and incubating diatoms and by several Fe fertilization experiments from southern, equatorial, and northern latitudes [*Cortese and Gersonde*, 2007, and references therein]. Fe stress causes diatoms to reduce their C and N content while simultaneously helps to increase the amount of Si in their cell walls, which in turn determines that Fe-limited diatoms have a higher Si:N ratio [*Hutchins and Bruland*, 1998; *Takeda*, 1998]. This results in greater consumption of Si compared to N in the modern low-Fe waters of the southern Agulhas Plateau. The potential for fertilization of Fe-limited waters depends on the source of this iron, with Fe supplied in the form of atmospheric dust more likely to be biologically available than Fe from other sources (lithogenic material transported by bottom currents or distal turbidites) [*Mortlock et al*., 1991; *Kumar et al*., 1995]. It is commonly argued that glacial increases of atmospheric dust input [*Lambert et al*., 2008] might have increased the bioavailability of dust-borne Fe [*Kumar et al*., 1995; *Mahowald et al*., 1999; *Kohfeld et al*., 2005]. The geochemical provenance of dust markers shows that the wind-transported lithogenics accumulated in Antarctica and Southern Ocean sediments eroded either from the exposed Argentinean shelf or by Patagonian ice fields that emptied directly into the Southern Ocean /South Atlantic [*Basile et al*., 1997] and represented a potential source of biologically available Fe [*Mahowald et al*., 1999; *Chase et al*., 2003; *Kohfeld et al*., 2005], which led to increases of biosiliceous productivity over site MD02-2588 during glacials for the past 350 kyr (Figure 3a). This interpretation is supported by the significantly higher paleoproductivity at site MD02-2588 under full glacial conditions (Figures 4d and 4c), which temporally match records from a wide area along the Atlantic sector of the Southern Ocean [*Mortlock et al*., 1991; *Kumar et al*., 1995]. Fe fertilization has been a recurrent feature of the sub-Antarctic region of the Atlantic sector during the Pleistocene, as records of dust/Fe input and marine export production closely correlate over short [*Mortlock et al*., 1991; *Kumar et al*., 1995] and long time spans [*Martínez-García et al*., 2009, 2014].

Much of the new production in Fe-rich areas of Southern Ocean and the South Atlantic is mediated by phytoplankton blooms dominated by fast-growing, spore-forming species of *Chaetoceros* that build up biomass until nitrate exhaustion [*Smetacek*, 1985; *Abelmann et al*., 2006]. Following nutrient exhaustion in surface waters, the contribution of vegetative cells of *Chaetoceros* converted into spores increases, which also induces rapid mass sinking of valves [*Smetacek*, 1985; *Romero and Armand*, 2010, and references therein]. In the bloom aftermath, *Chaetoceros* RS clump into rapidly sinking aggregates, which sequesters CO_2 into the ocean interior and down to the sediments [*Smetacek*, 1999]. Increased concentrations of *Chaetoceros* RS in a wide area of Atlantic sector of the Southern Ocean during the Last Glacial Maximum have been related to dust-mediated iron fertilization, upwelling, and icebergs breakup enhanced productivity [*Abelmann et al*., 2006]. Though it appears that diatoms with low uptake ratio of Si—such as *Chaetoceros*—also have a high dissolution rate [*Romero and Armand*, 2010], we postulate that the bloom-and-bust strategy of *Chaetoceros* vegetative cells in surface waters overlying site MD02-2588 strongly contributed to glacial maxima of total

diatom fluxes (Figure 3a) and the production and sedimentation of opal and organic matter (Figures 4a and 4b) in the southern Agulhas Plateau.

6.2. Front Migrations in the Southern Ocean and Diatom Production

Compared to its current position in the southern Agulhas Plateau, it has been proposed that the STF—considered to be the northern limit of SASW at ~39°–40°S [*Orsi et al*., 1995]—migrated northward between 4° [*Rau et al*., 2002] and 7° of latitude [*Bard and Rickaby*, 2009] during late Quaternary glacials. Following this scenario, it can be assumed that site MD02-2588—presently underneath the STF (Figure 1)—was bathed by SASW almost throughout glacials for the past 350 kyr. In addition to the high nutrient supply (see section 6.1), strong vertical mixing of the uppermost water column and low SST (Figure 4e) provided the physical conditions for enhanced diatom production during glacials in the southern Agulhas Plateau.

The dynamics of equatorward migration of the STF during the late Quaternary varied depending on the length and the severity of glacials. It has been proposed that colder-than-usual glacials (e.g., MIS12 [*Bard and Rickaby*, 2009]) exhibited a more equatorward displacement of the average position of the STF and, thus, affected the water transport from the Indian Ocean into the Indian-Atlantic Ocean gateway and beyond [*Peeters et al*., 2004; *Bard and Rickaby*, 2009; *Caley et al*., 2012]. The net transfer of surface and thermocline waters from the Indian Ocean around the southern African tip may alter as fronts migrate [*Gordon et al*., 1992; *Sloyan and Rintoul*, 2001]. Since resistance to dissolution is a common feature to both main diatom groups identified at site MD02-2588 (RS *Chaetoceros* and tropical/subtropical taxa), low-to-moderate values of tropical/subtropical diatoms—indicative of warmer, high-salinity waters (see section 4)—during MIS8, MIS6, MIS4, and MIS2 (Figure 3c) suggest that the southward advection of STSW over the southern Agulhas Plateau weakened during full glacials, though never completely shut off the Indian-Atlantic gateway along the South African tip for the past 350 kyr. According to the temporal variations of diatom groups at site MD02-2588 (Figures 3b–3d), the location of the STF at its northernmost position over the southern Agulhas Plateau occurred between the early and middle stages of full glacials, while it started to move southward well before terminations, potentially allowing increased leakage through the Indian Ocean surface flow. Since the magnitude and intensity of the transport flux of heat between the Indian and Atlantic Oceans play a crucial role in global ocean circulation, the onset of increased Agulhas leakage toward the late interglacials suggests a crucial role for Agulhas leakage in glacial terminations, timing of interhemispheric climate change, and the resulting resumption of the Atlantic meridional overturning circulation [*Peeters et al*., 2004; *Caley et al*., 2012].

The southward migration of the STF during full interglacials [*Flores et al*., 1999; *Rau et al*., 2002; *Peeters et al*., 2004; *Bard and Rickaby*, 2009; *Marino et al*., 2013; *Simon et al*., 2013; *Martínez-García et al*., 2014] led to the warming of surface waters over site MD02-2588 (Figure 4e) and enhanced the stratification of the uppermost ocean. Diatoms responded to the weakened mixing and the decreased nutrient supply in the southern Agulhas Plateau by reducing their total production during MIS9, MIS7, MIS5, and MIS1. Shifts in the species composition of the diatom assemblage (Figures 3b–3d) support our interpretation of nutrient and hydrographic changes. *Fragilariopsis doliolus* and accompanying species of the tropical/subtropical group (see section 4) tend to dominate the diatom community of low- to middle-latitude ocean waters during periods of productivity collapse following the shutdown of nutrient entrainment and the onset of stratification (review in *Romero and Armand* [2010]). The low biosiliceous productivity during MIS9, MIS7, MIS5, and MIS1 might have been additionally determined by a smaller Si supply to surface waters overlying the southern Agulhas Plateau. Substantial consumption of Si by diatoms and radiolarians thriving south of the PF during interglacials [*Brzezinski et al*., 2002; *Matsumoto et al*., 2002; *Abelmann et al*., 2006] was possibly a consequence of interglacial retreats of winter sea ice cover in Antarctica [*Gersonde et al*., 2003; *Crosta et al*., 2004] and the decreased eolian supply of nutrients to the Southern Ocean/South Atlantic [*Mortlock et al*., 1991; *Kumar et al*., 1995; *Kohfeld et al*., 2005]. Alternatively, a less efficient Si utilization by diatoms north of the PF [*Chase et al*., 2003] might have occurred. Since the species-specific composition of the tropical/subtropical assemblage at site MD02-2588 barely varied among interglacials throughout the last 350 kyr, the scenario of inefficient Si utilization seems therefore less plausible.

Superimposed on the glacial-interglacial pattern of variability, suborbital-scale variations of alkenone concentration and SST (Figures 4d and 4e) and the simultaneous occurrence of both main diatom groups suggest that the STF and associated water masses migrated back and forth over site MD02-2588 on millennial

timescales. Independent of the orbital-scale pattern of latitudinal migrations of the STF, the millennial and submillennial variations of its average location translated into rapid variations of salinity and SST features of the uppermost waters overlying site MD02-2588. In their reconstruction of late Pleistocene Agulhas leakage record at site MD02-2588, *Marino et al*. [2013] recognized prominent millennial-scale variations of the foraminera-based Mg/Ca temperature signal for the interval 265–75 kyr. Since surface waters north of the Agulhas Return Current have their origins in the subtropical gyre of the Indian Ocean [*Gordon et al*., 1992; *Sloyan and Rintoul*, 2001], the millennial-scale of variability of the STF latitudinal migrations also suggests short timescale contractions of subtropical gyres [*Sijp and England*, 2008; *De Deckker et al*., 2012; *Simon et al*., 2013] and the buildup of heat from the return flow that could not escape to the Atlantic [*Caley et al*., 2012].

6.3. The Last Four Terminations in the Southern Agulhas Plateau: Southern Versus Northern Hemisphere Forcing

A closer look at the last four terminations of the MD02-2588 record allows a better understanding of the processes and mechanisms behind variations of diatom productivity and SST variations that occurred during glacial-interglacial transitions in the southern Agulhas Plateau. On the basis of our multiparameter approach (Figure 5), we infer that each of TIV to TI displayed a largely similar pattern of events regarding nutrient availability, water temperature, and water masses dynamics. Diatom production and SST, however, varied strongly close to the begin and during Terminations.

A striking feature common to all last four glacial culminations at site MD02-2588 is the good match between high total diatom values and high percentages of RS *Chaetoceros* (Figures 5a and 5b) with the enhanced dust values of the EPICA record (Figure 5c). This match seems to be stronger during T1 (highest total diatom concentrations matches strongest dust input). Assuming a mechanistic link between bioavailable Fe fertilization and diatom production [*Hutchins and Bruland*, 1998; *Takeda*, 1998] in the southern Agulhas Plateau, we speculate that the substantial diatom increase toward the end of MIS2 was the rapid response of diatoms to strong increase of atmospheric dust/bioavailable Fe input into the low-latitude South Atlantic (see also section 6.1). Although dust deposition depends on wind patterns and intensity, scavenging of dust particles by precipitation and the extension of dust source areas [*Mahowald et al*., 1999], the lower eolian input into the Southern Ocean/South Atlantic during TIV, TIII, and TII (Figure 5c) [*Kohfeld et al*., 2005] is proposed as one of the main causes of lower diatom production due to lessened Fe bioavailability in surface waters of the southern Agulhas Plateau.

Since *F. kerguelensis* is eurythermal (1–13°C and, hence, below the SST values for the glacial-interglacial transitions at site MD02-2588), we argue that its increased contribution during terminations (Figure 5f) represents a transport rather than an in situ production signal. Considered to be endemic to Southern Ocean waters, *F. kerguelensis* dominates the diatom assemblage of the open ocean zone south of the PF and reaches up to 80% of the total assemblage preserved in surface sediments between the winter sea ice edge and the SAF (see section 4) [*Crosta et al*., 2005, and references therein]. The good match between the rapid increases of *F. kerguelensis* and warmings recorded in the Vostok δD record (Figures 5e and 5f) suggests pulses of northward transport of southern originated waters. *Bianchi and Gersonde* [2002] reported significant hydrographic changes south of the PF by the latest MIS6: SST warmed and, relative to its modern position, the PF shifted southward by 3° to 5° of latitude. The southward retreat of the Antarctica winter sea ice cover, the breakup of extensive ice shelves, and the SST warming south of the PF resulted in dramatic changes of the environmental conditions north of the PF at the time [*Bianchi and Gersonde*, 2002]. These events, related to the impact of high-latitude summer insolation [*Bianchi and Gersonde*, 2002], led to meltwater spikes at the beginning of TII, which might have triggered high *F. kerguelensis* production south of the PF followed by enhanced northward transport of its valves.

Compared to low Si:N ratios of RS *Chaetoceros* [*Smetacek*, 1985], the high Si:N (approximately 2–6) of *F. kerguelensis* translates into thick, resistant valves whose Si deposition rates are not slowed by low Fe availability [*Hutchins and Bruland*, 1998; *Takeda*, 1998]. In contrast to the high organic matter supplied by RS *Chaetoceros* [*Smetacek*, 1999; *Abelmann et al*., 2006], the amount of accumulated organic matter (Figure 4c) provided by well-silicified frustules of *F. kerguelensis* at site MD02-2588 was almost negligible. The selective removal of Si from surface waters during glacial culminations occurred without diatoms reaching bloom proportions (such as during full glacials) and resulted in gradual Si depletion relative to N and P over site MD02-2588. As a consequence of the larger availability of N and P, phytoplankton populations in surface waters over site MD02-2588 shifted into a more calcareous-dominated community toward early interglacials.

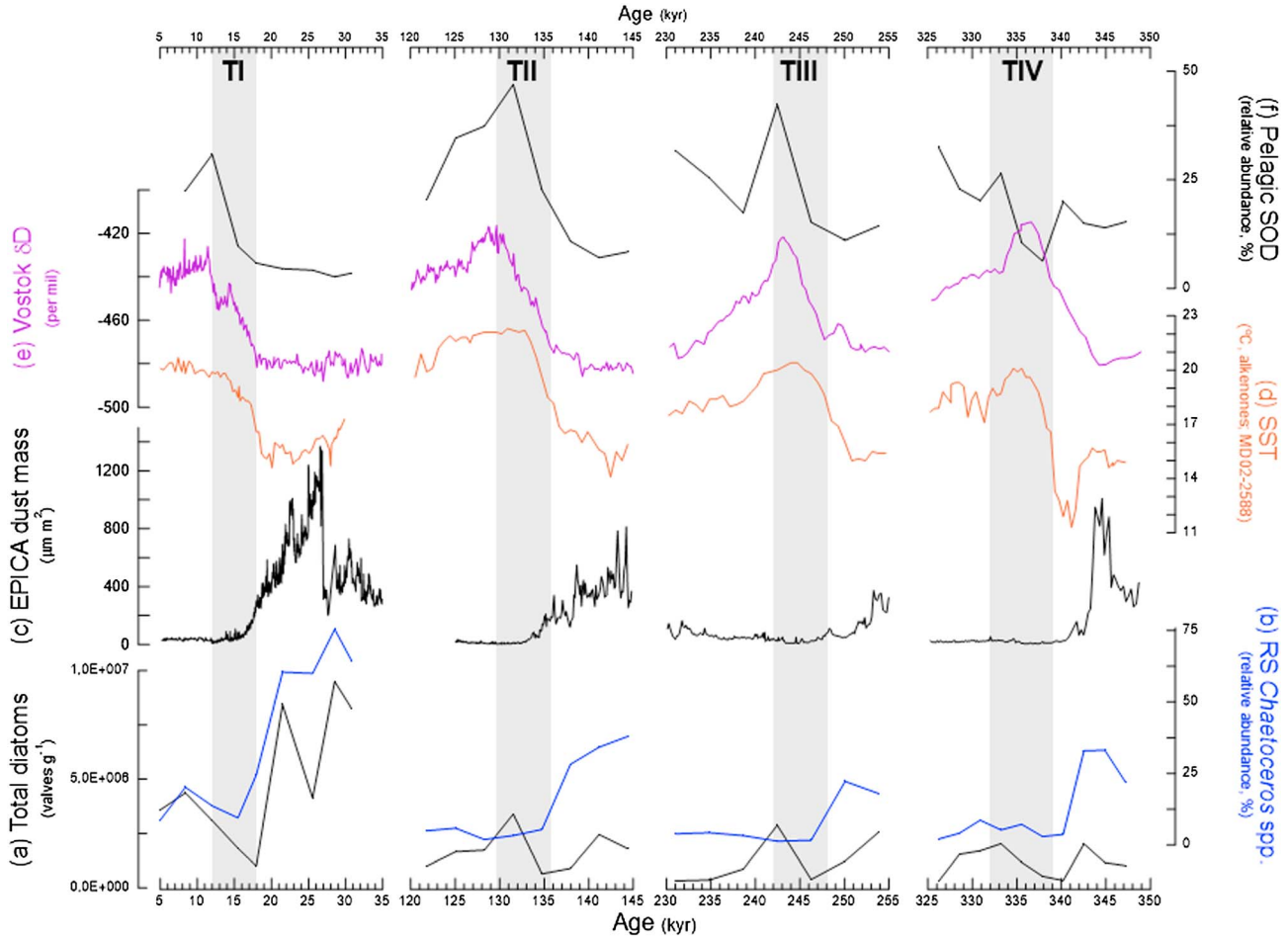

Figure 5. Comparison of paleoclimate and paleoceanographic records from the Souhtern Ocean and the southern Agulhas Plateau for Terminations IV to I (vertical grey shadings). Records include (a) total diatom concentration (valves g^{-1}, black line, MD02-2588), (b) RS *Chaetoceros* (relative abundance, %, blue line, MD02-2588), (c) EPICA dust record ($\mu m\ m^{-2}$, black line) [*Lambert et al*., 2008], (d) alkenone-based SST (°C, light orange line, MD02-2588), (e) Vostok δD record (wt %, purple line) [*Petit et al*., 1999], and (f) pelagic Southern Ocean diatoms (SOD, relative abundance, %, black line, MD02-2588). Reference: T = terminations.

Two common features of the SST record for the transition from glacial conclusions into TIV to TI are major millennial-scale oscillations and a rapid warming, which lasted each less than 6000 years (Figure 5d). A similar amplitude of Mg-Ca-reconstructed SST increases at site MD02-2588 during TIII and TII has been recorded [*Marino et al*., 2013]. The high temporal resolution of our SST record allows for a detailed comparison with Antarctic ice core climate records. Temperature amplitudes across TIV to TI are higher in the Vostok δD record (which records air temperature changes over Antarctica [*Petit et al*., 1999]) than in our alkenone-derived SST (Figures 5d and 5e). Except during TIV, the rise of SST started earlier at site MD02-2588 than in the Vostok δD record. This discrepancy is interpreted to be indicative of strong glacial coolings of Antarctic air in connection with increased thermal isolation due to enhanced circum-Antarctic circulation [*Cortese et al*., 2007]. The leads of the MD02-2588 SST record over the Vostok record, already known from low, middle, and high latitudes [*Cortese et al*., 2007, and references therein], suggest that the early warming of the uppermost surface waters overlying site MD02-2588 before any considerable (Antarctic) ice volume change occurred and support the scenario of a Northern Hemisphere lead in the generation of the SST signal in the southern Agulhas Plateau.

7. Conclusions

Our multiparameter approach suggests that the latitudinal migration of the South Atlantic/Southern Ocean fronts and the resulting latitudinal shifts in nutrient availability play a decisive role in the pattern of variations of diatom and bulk content in the southern Agulhas Plateau. The good match between high biosiliceous

productivity, winter Antarctic sea ice cover, and dust/Fe input suggests that the leakage of preformed Si and dust-induced Fe fertilization actively drove Si uptake by diatoms over site MD02-2588 during the past 350 kyr. The high sensitivity of the biological pump to Fe fertilization has important implications for the coupling between atmospheric dust flux and diatom paleoproductivity in front zones of the midlatitude world ocean.

The high contribution of spores of *Chaetoceros* during MIS2–MIS4 and MIS6 is a compelling evidence for substantially northward migration of the STF and the associated SASW. The N-S migrations of the Southern Ocean/South Atlantic fronts influenced diatom productivity by transporting Si closer to site MD02-2588. Moderate contributions of tropical/subtropical diatoms during glacials suggest that equatorward displacements of the STF did not entirely obstruct the leakage from Indian Ocean waters into the Indian-Atlantic Ocean gateway.

Glacial culminations (the interval previous to each termination) at site MD02-2588 were characterized by moderate (TIV to II) to high (TI) diatom productivity, low SST, and weak stratification of the uppermost water column. The rapid increase of *F. kerguelensis* at site MD02-2588 during the last four terminations represents a transport signal of Antarctic origin and contributed less to opal and organic matter content. The lead of the alkenone-based SST at site MD02-2588 during TIII, II, and I over Antarctic air temperatures (Vostok record) points to the warming of surface waters of the southern Agulhas Plateau before changes in Antarctic ice sheets occurred.

Our multiparameter approach shows that the transfer mechanisms of orbital- and suborbital-scale climate variations in the southern Agulhas Plateau during the past 350 kyr were mixed: glacial rises of diatom productivity were mainly Southern Hemisphere driven by inputs of dust/Fe (atmosphere) and Si (hydrography), while SST variations (climate) were mainly driven by the Northern Hemisphere.

Acknowledgments

We thank the officers and crew of the RV *Marion Dufresne* for their technical support enabling the recovery of MD02-2588. M. Klann (MARUM, Bremen, Germany) is acknowledged for the opal measurements. This work was partially funded by the Deutsche Forschungsgemeinschaft (OER), the UK Natural Environment Research Council (NERC and the Seventh Framework Programme PEOPLE Work Programme grant 238512 (Marie Curie Initial Training Network "GATEWAYS")). J.-H.K. acknowledges that in part the research leading to these results has received funding from the European Research Council under the European Union's Seventh Framework Programme (FP7/2007-2013)/ERC grant agreement (226600). Comments and suggestions by two anonymous reviewers greatly improved a first version of this work. Data are available in the database www.pangaea.de.

References

Abelmann, A., R. Gersonde, G. Cortese, G. Kuhn, and V. Smetacek (2006), Extensive phytoplankton blooms in the Atlantic sector of the glacial Southern Ocean, *Paleoceanography*, *21*, PA1013, doi:10.1029/2005PA001199.

Armand, L. K., X. Crosta, O. E. Romero, and J.-J. Pichon (2005), The biogeography of major diatom taxa in Southern Ocean sediments: 1. Sea ice related species, *Palaeogeogr. Palaeoclimatol. Palaeoecol.*, *223*, 93–126.

Bard, E., and R. E. M. Rickaby (2009), Migration of the subtropical front as a modulator of glacial climate, *Nature*, *460*, 380–383, doi:10.1038/nature08189.

Basile, I., F. E. Grousset, M. Revel, J. R. Petit, P. E. Biscaye, and N. I. Barkov (1997), Patagonian origin of glacial dust deposited in East Antarctica (Vostok and Dome C) during glacial stages 2, 4, and 6, *Earth Planet. Sci. Lett.*, *146*, 573–589.

Belkin, I. M., and A. L. Gordon (1996), Southern Ocean fronts from the Greenwich meridian to Tasmania, *J. Geophys. Res.*, *101*, 3675–3696, doi:10.1029/95JC02750.

Bianchi, C., and R. Gersonde (2002), The Southern Ocean surface between Marine Isotope Stages 6 and 5d: Shape and timing of climatic changes, *Palaeogeogr. Palaeoclimatol. Palaeoecol.*, *197*, 151–177.

Bryden, H. L., and L. M. Beal (2001), Role of the Agulhas Current in Indian Ocean circulation and associated heat and freshwater fluxes, *Deep Sea Res., Part I*, *48*, 1821–1845.

Brzezinski, M. A., C. J. Pride, V. M. Franck, D. M. Sigman, J. L. Sarmiento, K. Matsumoto, N. Gruber, G. H. Rau, and K. H. Coale (2002), A switch from $Si(OH)_4$ to NO_3 depletion in the glacial Southern Ocean, *Geophys. Res. Lett.*, *29*(12), 1564, doi:10.1029/2001GL014349.

Caley, T., et al. (2012), High-latitude obliquity as a dominant forcing in the Agulhas current system, *Clim. Past*, *7*, 1285–1296, doi:10.5194/cp-1287-1285-2011.

Chase, Z., R. F. Anderson, M. Q. Fleisher, and P. W. Kubik (2003), Accumulation of biogenic and lithogenic material in the Pacific sector of the Southern Ocean during the past 40,000 years, *Deep Sea Res., Part II*, *50*, 799–832.

Cortese, G., and R. Gersonde (2007), Morphometric variability in the diatom *Fragilariopsis kerguelensis*: Implications for Southern Ocean paleoceanography, *Earth Planet. Sci. Lett.*, *257*, 526–544.

Cortese, G., A. Abelmann, and R. Gersonde (2007), The last five glacial-interglacial transitions: A high-resolution 450,000-year record from the subantarctic Atlantic, *Paleoceanography*, *22*, PA4203, doi:10.1029/2007PA001457.

Crosta, X., A. Sturm, L. Armand, and J.-J. Pichon (2004), Late Quaternary sea ice history in the Indian sector of the Southern Ocean as recorded by diatom assemblages, *Mar. Micropaleontol.*, *50*, 209–223.

Crosta, X., O. E. Romero, L. K. Armand, and J.-J. Pichon (2005), The biogeography of major diatom taxa in Southern Ocean sediments: 2. Open-ocean related species, *Palaeogeogr. Palaeoclimatol. Palaeoecol.*, *223*, 66–92.

De Deckker, P., M. Moros, K. Perner, and E. Jansen (2012), Influence of the tropics and southern westerlies on glacial interhemispheric asymmetry, *Nat. Geosci.*, *5*, 266–269, doi:10.1038/NGEO1431.

De Master, D. J. (1981), The supply and accumulation of silica in the marine environment, *Geochim. Cosmochim. Acta*, *45*, 1715–1732.

Diz, P., I. R. Hall, R. Zahn, and E. G. Molyneux (2007), Paleoceanography of the southern Agulhas Plateau during the last 150 ka: Inferences from benthic foraminiferal assemblages and multispecies epifaunal carbon isotopes, *Paleoceanography*, *22*, PA4218, doi:10.1029/2007PA001511.

Fischer, G., R. Gersonde, and G. Wefer (2002), Organic carbon, biogenic silica and diatom fluxes in the marginal winter sea-ice zone and in the Polar Front Region: Interannual variations and differences in composition, *Deep Sea Res., Part II*, *49*, 1721–1745.

Flores, J.-A., R. Gersonde, and F. J. Sierro (1999), Pleistocene fluctuations in the Agulhas Current Retroflection based on the calcareous plankton record, *Mar. Micropaleontol.*, *37*, 1–22.

Gersonde, R., et al. (2003), Last glacial seas surface temperatures and sea-ice extent in the Southern Ocean (Atlantic-Indian sector): A multiproxy approach, *Paleoceanography*, *18*(3), 1061, doi:10.1029/2002PA000809.

Gordon, A. L., J. R. E. Lutjeharms, and M. K. Gründlingh (1987), Stratification and circulation at the Agulhas Retroflection, *Deep Sea Res., Part I*, *34*, 565–599.
Gordon, A. M., R. F. Weiss, W. M. Smethie Jr., and M. J. Warner (1992), Thermocline and intermediate water communication between the South Atlantic and Indian Oceans, *J. Geophys. Res.*, *97*, 7223–7240, doi:10.1029/92JC00485.
Graham, R. M., and A. M. De Boer (2013), The dynamical subtropical front, *J. Geophys. Res. Oceans*, *118*, 5676–5685, doi:10.1002/jgrc.20408.
Holliday, N. P., and J. F. Read (1998), Surface oceanic fronts between Africa and Antarctica, *Deep Sea Res., Part I*, *45*, 217–238.
Hutchins, D. A., and K. Bruland (1998), Iron-limited diatom growth and Si:N uptake ratios in a coastal upwelling regime, *Nature*, *393*, 561–564.
Kim, J.-H., R. R. Schneider, P. J. Müller, and G. Wefer (2002), Interhemispheric comparison of deglacial sea-surface temperature patterns in Atlantic eastern boundary currents, *Earth Planet. Sci. Lett.*, *194*, 383–393.
Kohfeld, K. E., C. Le Quéré, S. P. Harrison, and R. F. Anderson (2005), Role of marine biology in glacial-interglacial CO_2 cycles, *Science*, *308*, 74–78.
Kumar, N., R. F. Anderson, R. A. Mortlock, P. N. Froelich, P. Kubik, B. Dittrich-Hannen, and M. Suter (1995), Increased biological productivity and export production in the glacial Southern Ocean, *Nature*, *378*, 675–380.
Lambert, P., B. Delmonte, J. R. Petit, M. Bigler, P. R. Kaufmann, M. A. Hutterli, T. F. Stocker, U. Ruth, J. P. Steffensen, and V. Maggi (2008), Dust-climate couplings over the past 800,000 years from the EPICA Dome C ice core, *Nature*, *453*, 613–619.
Lisiecki, L. E., and M. E. Raymo (2005), A Pliocene-Pleistocene stack of 57 globally distributed benthic $\delta^{18}O$ records, *Paleoceanography*, *20*, PA1003, doi:10.1029/2004PA001071.
Lutjeharms, J. R. E. (1996), The exchange of water between the South Indian and South Atlantic Oceans, in *The South Atlantic: Present and Past Circulation*, edited by G. Wefer et al., pp. 125–162, Springer, Berlin.
Mahowald, N., K. Kohfeld, M. Hansson, Y. Balkanski, S. P. Harrison, I. C. Prentice, M. Schulz, and H. Rodhe (1999), Dust sources and deposition during the last glacial maximum and current climate: A comparison of model results with paleodata from ice cores and marine sediments, *J. Geophys. Res.*, *104*, 15,895–15,916, doi:10.1029/1999JD900084.
Marino, G., R. Zahn, M. Ziegler, C. Purcell, G. Knorr, I. R. Hall, P. Ziveri, and H. Elderfield (2013), Agulhas salt-leakage oscillations during abrupt climate changes of the Late Pleistocene, *Paleoceanography*, *28*, 599–606, doi:10.1002/palo.20038.
Martin, J. H. (1990), Glacial-interglacial CO_2 change: The iron hypothesis, *Paleoceanography*, *5*, 1–13, doi:10.1029/PA005i001p00001.
Martínez-García, A., A. Rosell-Melé, W. Geibert, R. Gersonde, P. Masqué, V. Gaspari, and C. Barbante (2009), Links between iron supply, marine productivity, sea surface temperature, and CO_2 over the last 1.1 Ma, *Paleoceanography*, *24*, PA1207, doi:10.1029/2008PA001657.
Martínez-García, A., D. M. Sigman, H. Ren, R. F. Anderson, M. Straub, D. A. Hodell, S. L. Jaccard, T. I. Eglinton, and G. H. Haug (2014), Iron fertilization of the Subantarctic Ocean during the Last Ice Age, *Science*, *343*, 1347–1350.
Martínez-Méndez, G., R. Zahn, I. R. Hall, F. J. C. Peeters, L. D. Pena, I. Cacho, and C. Negre (2010), Contrasting multiproxy reconstructions of surface ocean hydrography in the Agulhas Corridor and implications for the Agulhas Leakage during the last 345,000 years, *Paleoceanography*, *25*, PA4227, doi:10.1029/2009PA001879.
Matano, R. P., C. G. Simionato, and P. T. Strub (1999), Modeling the wind-driven variability of the south Indian Ocean, *J. Phys. Oceanogr.*, *29*, 217–230.
Matsumoto, K., J. Sarmiento, and M. A. Brzezinski (2002), Silicic acid leakage from the Southern Ocean: A possible explanation for glacial atmospheric pCO_2, *Global Biogeochem. Cycles*, *16*(3), 1031, doi:10.1029/2001GB001442.
Molyneux, E. G., I. R. Hall, R. Zahn, and P. Diz (2007), Deep water variability on the southern Agulhas Plateau: Interhemispheric links over the past 170 ka, *Paleoceanography*, *22*, PA4209, doi:10.1029/2006PA001407.
Mortlock, R. A., C. D. Charles, P. N Froelich, M. A. Zibello, J. Saltzmann, J. D. Hays, and L. H. Burckle (1991), Evidence for lower productivity in the Antarctic Ocean during the last Glaciation, *Nature*, *35*, 220–223.
Müller, P., and R. R. Schneider (1993), An automated leaching method for the determination of opal in sediments and particulate matter, *Deep Sea Res., Part I*, *40*, 425–444.
Müller, P. J., R. R. Schneider, and G. Ruhland (1994), Late Quaternary PCO_2 variations in the Angola Current: Evidence from organic carbon $\delta^{13}C$ and alkenone temperature, in *Carbon Cycling in the Glacial Ocean: Constraints on the Ocean's Role in Global Change*, *NATO ASI Ser. I*, edited by R. Zahn et al., pp. 343–366, Springer, Berlin.
Müller, P., G. Kirst, G. Ruhland, I. von Storch, and A. Rosell-Melé (1998), Calibration of the alkenone paleotemperature index $U^{K'}_{37}$ based on core-tops from the eastern South Atlantic and the global ocean (60°N–60°S), *Geochim. Cosmochim. Acta*, *62*, 1757–1772.
Orsi, A. H., T. Whitworth III, and W. D. Nowlin Jr. (1995), On the meridional extent and fronts of the Antarctic Circumpolar Current, *Deep Sea Res., Part I*, *42*, 641–673.
Peeters, F. J. C., R. Acheson, G.-J. A. Brummer, W. P. M. de Ruijter, R. R. Schneider, G. M. Ganssen, E. Ufkes, and D. Kroon (2004), Vigorous exchange between the Indian and Atlantic oceans at the end of the past five glacial periods, *Nature*, *430*, 661–665.
Peterson, R. G., and L. Stramma (1991), Upper-level circulation in the South Atlantic Ocean, *Prog. Oceanogr.*, *26*, 1–73.
Petit, J. R., et al. (1999), Climate and atmospheric history of the past 420,000 years from the Vostok Ice Core, Antarctica, *Nature*, *399*, 429–436.
Prahl, F. G., and S. G. Wakeham (1987), Calibration of unsaturation patterns in long-chain ketone compositions for paleotemperature assessment, *Nature*, *330*, 367–369.
Prahl, F. G., L. A. Muehlhausen, and D. L. Zahnle (1988), Further evaluation of long-chain alkenones as indicators of paleoceanographic conditions, *Geochim. Cosmochim. Acta*, *52*, 2303–2310.
Rau, A. J., J. Rogers, J. R. E. Lutjeharms, J. Giraudeau, J. A. Lee-Thorp, M.-T. Chen, and C. Waelbroeck (2002), A 450-kyr record of hydrological conditions on the western Agulhas Bank Slope, south of Africa, *Mar. Geol.*, *180*, 183–201.
Read, J. F., M. I. Lucas, S. E. Holley, and R. T. Pollard (2000), Phytoplankton, nutrients and hydrography in the frontal zone between the Southwest Indian Subtropical gyre and the Southern Ocean, *Deep Sea Res., Part I*, *47*, 2341–2368.
Romero, O. E., and L. K. Armand (2010), Marine diatoms as indicators of modern changes in oceanographic conditions, in *The Diatoms, Applications for the Environmental and Earth Sciences*, 2nd ed., edited by J. P. Smol and E. F. Stoermer, pp. 373–400, Cambridge Univ. Press, Cambridge, U. K.
Romero, O. E., L. K. Armand, X. Crosta, and J.-J. Pichon (2005), The biogeography of major diatom taxa in Southern Ocean sediments: 3. Tropical/subtropical species, *Palaeogeogr. Palaeoclimatol. Palaeoecol.*, *223*, 49–65.
Sarmiento, J. L., N. Gruber, M. A. Brzezinski, and J. P. Dunne (2004), High-latitude controls of thermocline nutrients and low latitude biological productivity, *Nature*, *427*, 56–60.
Schlitzer, R. (2002), Carbon export fluxes in the Southern Ocean: Results from inverse modeling and comparison with satellite-based estimates, *Deep Sea Res., Part II*, *49*, 1623–1644.
Schrader, H.-J., and R. Gersonde (1978), Diatoms and silicoflagellates, in *Micropaleontological Counting Methods and Techniques—An Exercise on an Eight Meter Section of the Lower Pliocene of Capo Rosello, Sicily*, *Utrecht Micropaleontol. Bull.*, vol. 17, edited by W. J. Zachariasse et al., pp. 129–176, Loonzetterij Abé, Hoogeveen, Netherlands.
Sigman, D. M., M. A. Altabet, R. Francois, D. C. McCorkle, and J. F. Gaillard (1999), The isotopic composition of diatom bound nitrogen in Southern Ocean sediments, *Paleoceanography*, *14*, 118–134, doi:10.1029/1998PA900018.

Sijp, W., and M. H. England (2008), The effect of a northward shift in the southern hemisphere westerlies on the global ocean, *Prog. Oceanogr.*, *79*, 1–19.
Simon, M. H., K. L. Arthur, I. R. Hall, F. J. C. Peeters, B. R. Loveday, S. Barker, M. Ziegler, and R. Zahn (2013), Millennial-scale Agulhas Current variability and its implications for salt-leakage through the Indian-Atlantic Ocean gateway, *Earth Planet. Sci. Lett.*, *383*, 101–112.
Sloyan, B. M., and S. R. Rintoul (2001), Circulation, renewal, and modification of Antarctic mode and intermediate water, *J. Phys. Oceanogr.*, *31*, 1005–1030.
Smetacek, V. (1985), Role of sinking in diatom life-history cycles: Ecological, evolutionary and geological significance, *Mar. Biol.*, *84*, 239–251.
Smetacek, V. (1999), Diatoms and the ocean carbon cycle, *Protist*, *150*, 25–32.
Takeda, S. (1998), Influence of iron availability on nutrient consumption ratio of diatoms in oceanic waters, *Nature*, *393*, 774–777.
Taylor, J. R., and R. Ferrari (2011), Ocean fronts trigger high latitude phytoplankton blooms, *Geophys. Res. Lett.*, *38*, L23601, doi:10.1029/2011GL049312.
Uenzelmann-Neben, G. (2002), Seismic characteristics of sediment drifts: An example from the Agulhas Plateau, southwest Indian Ocean, *Mar. Geophys. Res.*, *22*, 323–343.
Ziegler, M., P. Diz, I. R. Hall, and R. Zahn (2013), Millennial-scale changes in atmospheric CO_2 levels linked to the Southern Ocean carbon isotope gradient and dust flux, *Nat. Geosci.*, *6*, 457–461.
Zielinski, U., and R. Gersonde (1997), Diatom distribution in Southern Ocean surface sediments (Atlantic sector): Implications for paleoenvironmental reconstructions, *Palaeogeogr. Palaeoclimatol. Palaeoecol.*, *129*, 213–250.